

Using circular economy principles to recycle materials in guiding the design of a wet scrubber-reactor for indoor air disinfection from coronavirus and other pathogens

Andrei Shishkin¹, Gaurav Goel^{2,3*}, Janis Baronins⁴, Jurijs Ozolins¹,
Clare Hoskins⁵ and Saurav Goel^{2,3,6}

¹ Rudolfs Cimdins Riga Biomaterials Innovations and Development Centre of RTU, Institute of General Chemical Engineering, Faculty of Materials Science and Applied Chemistry, Riga Technical University, LV-1007, Riga, Latvia.

² School of Engineering, London South Bank University, SE1 0AA, UK

³ School of Aerospace, Transport & Manufacturing, Cranfield University, MK43 0AL, UK

⁴ Maritime Transport department, Latvian Maritime Academy, 12, k-1, Flotes Str., Riga, LV-1016, Latvia

⁵ Pure and Applied Chemistry, University of Strathclyde, Glasgow, G1 1RD, UK

⁶ Department of Mechanical Engineering, Shiv Nadar University, Gautam Budh Nagar, 201314, India

*Corresponding author Email: goelg@lsbu.ac.uk

Abstract

An arduous need exists to discover rapid solutions to avoid the accelerated spread of coronavirus especially through the indoor environments like offices, hospitals, and airports. One such measure could be to disinfect the air, especially in indoor environments. The goal of this work is to propose a novel design of a wet scrubber-reactor to deactivate airborne microbes using circular economy principles. Based on Fenton's reaction mechanism, the system proposed here will deactivate airborne microbes (bioaerosols) such as SARS-CoV-2. The proposed design relies on using a highly porous clay-glass open-cell structure as an easily reproducible and cheap material. The principle behind this technique is an in-situ decomposition of hydrogen peroxide into highly reactive oxygen species and free radicals. The high porosity of a tailored ceramic structure provides a high contact area between atomized oxygen, free radicals and supplied polluted air. The design is shown to comply with the needs of achieving sustainable development goals.

Keywords: Air disinfection; Scrubber-reactor; Coronavirus; Preparedness, Porous ceramics, COVID-19

1. Introduction

Severe Acute Respiratory Syndrome CoronaVirus 2 (SARS-CoV-2) is the recently discovered etiological agent of the COVID-19 (Singh et al., 2020), the emergence of which led to a pandemic outbreak in 2020. Delayed reactions and wrong conclusions drawn from a preliminary investigations on COVID-19 resulted in a lockdown of more than 2 billion people globally, affecting social and economic activities at an unprecedented scale which has brought us to a state of global recession (Shalal and Lawder, 2020).

The rapid spread of COVID-19 disease has enforced emergent and agile research actions to develop control measures. It has been shown that SARS CoV-2, the virus causing the COVID-19 disease is stable on plastic surfaces (such as on personal protective equipment and face mask) for up to seven days and up to 3 hours or even longer in aerosol form (airborne) (Bourouiba, 2020; Morawska et al., 2020; Prather et al., 2020). This stability puts medical professionals and people commuting in public transport at great risk of infection (Goldberg et al., 2021; Nissen et al., 2020). One of the mechanisms to stop the spread of COVID-19 in an indoor environment will be to continuously filter the air surrounding us to avoid the risk of accidental inhalation or ingestion of the virus and any other pathogen (Morawska et al., 2020).

Unfortunately, the currently available commercial air filters are susceptible for plugging during passage of high particulate matter loaded air (Liu et al., 2017) and are not designed to passivate a virus like SARS-CoV-2. These air filters may become potential source for the spread of microbes as they accumulate particulate matter and virus attached to them during the filtration process. Collected and incubated bacteria and viruses can be released by the penetration process during maintenance of the air scrubbing system (e.g., leakage during removal of packing material) (Di Natale et al., 2018). These commercial filters lack an efficient mechanism for killing the harmful microbes. Therefore, there is an urgent need to design air filters for deactivating microbes (i.e., bacteria and viruses). Such systems need to be simple by design and cheaper in price to make it affordable for everyone in the society.

Clay is the most widespread natural material and hence is easily available, offering the possibility to meet these requirements and was therefore tested for the design of the filter proposed here. Also, hydrogen peroxide (H_2O_2) was combined to exploit the well-known Fenton’s reaction (Fenton, 1894) thus killing all the microbes via production of reactive oxygen species (ROS) and free radical generation. The use of hydrogen peroxide against coronavirus has already been approved by the United States Food and Drug Administration (FDA, 2020) and is recommended in other studies (Goel et al., 2020a; Kampf et al., 2020). The *in-situ* decomposition of H_2O_2 disinfects the air stream using its production of reactive oxygen species. The highly oxidised crystalline phase of glass-clay ceramics exhibits high stability towards such chemicals. Hence, this approach will result in the filtered air, containing a relatively high moisture content, which will be free from biologically hazardous contaminants. Any ceramic foam production method can be used for this purpose (i.e., kaolinite or bentonite type clay foam). Most such systems will have high porosity along with uniform distribution of a catalyst (e.g., Fe_2O_3 content or Al_2O_3). Some types of clays like the illite-type are naturally rich in Fe_2O_3 and will automatically provide the catalyst presence required to initiate the Fenton reaction resulting in the degradation of H_2O_2 . This is the hypothesis tested in this crucial first phase of the work.

Thus, development of an agile engineering solution to suppress the spread of coronavirus (SARS-CoV-2) was the prime motive of this work. We based this research on an assumption that through exploitation of the Fenton reaction, we will be able to eliminate the SARS-CoV-2 virus and other pathogens during the air filtration. Some key research questions we addressed were:

- (i) Can a new approach be adopted to design an indoor air filter without getting plugged by the microbes during its continuous operation?
- (ii) Can the proposed use of highly porous ceramic foam capable of decomposing hydrogen peroxide into free radicals be an efficient strategy behind air disinfection from the coronavirus?
- (iii) What components of the filter system are needed and what connected knowledge is required for the integration of these components to adhere to the conditions required to promote the Fenton’s reaction (Fenton, 1894)?

2. Literature review

2.1. The evolution of pandemic due to COVID-19

It is believed that the lack of safety measures in wet markets caused a zoonotic transfer triggering the first episode with subsequent transmission of the coronavirus from animals to human beings (Andersen et al., 2020; Walsh and Cotovio, 2020; Zhou et al., 2020) and widespread global human spread. Studies suggest the source could be either RaTG13 from the *Rhinolophus affinis bat*, pangolin (*Manis javanica*) or a mix of these (i.e. zoonotic transfer) (Andersen et al., 2020; Hassanin, 2020). Genetic diversity has been discovered during recent genetic analysis, indicating the rapid evolution of the SARS-CoV-2. A total of up to ninety-three mutations and deletions on coding and non-coding deoxyribonucleic acid (DNA) regions have been found in eighty-six complete or nearly-complete samples of SARS-CoV-2 genomes (Phan, 2020). Three observed mutations were found located in the spike surface glycoprotein (S-Protein). These mutations might induce conformational changes and can play an essential role in binding to receptors on the host cell. Such property determines host tropisms, leading to possible changing antigenicity (Phan, 2020) and this may be the reason for the current non-seasonality of the virus (National Academies of Sciences, 2020). SARS CoV-2 primarily attacks the respiratory system, however, studies suggest that the human digestion system is also affected, with traces being noticed in the sewage system (Goel et al., 2020a; Mallapaty, 2020; Mao et al., 2020). The World Health Organisation (WHO) has released their data regarding stability and resistance of SARS-CoV-2, indicating its stability in human urine and faeces for up to 4 days (at higher pH than normal stool) (van Doremalen et al., 2020). However, heat at 56 °C efficiently eliminates the virus, at around 10,000 units of the SARS CoV-2 per 15 min which can be explained by the thermal aggregation of the membrane protein (Lee et al., 2005).

The spread of this pandemic may reoccur in the future due to continued close human involvement with wildlife, either due to their rearing for consumption or due to other events (e.g., forest fires, indirect land-use change, and the expansion of the urban environment) and the newer strains recently reported to be found in the UK (lineage B.1.1.7), Brazil (P.1), and South Africa (B.1.351) leading to a possible second, third and subsequent waves. Uncertainty surrounding the spread of SARS-CoV-2 is another issue that caught the Governments around the world off guard (CDC, 2020; Greenfieldboyce, 2020). Lack of preparedness to contain the spread of COVID-19 has resulted in deaths of above 2.3 million people globally already as on 05th February 2021 (Worldometer, 2021) and this number will continue to grow over time despite the vaccine campaign currently running worldwide. Although vaccine rollout is being made but the virus is rapidly evolving with new

mutations. This mandates the practice of basic hygiene, social distancing, and wearing of mask at public places to avoid the further spread. Efforts of face mask development have also been reported (Martí et al., 2021).

Studies have been conducted on the transmission dynamics of virus concerning indoor and outdoor spaces (Belosi et al., 2021; Coccia, 2020a, 2020b; Morawska and Cao, 2020; Noorimotlagh et al., 2021) and also interaction between air pollution and meteorological factors, including wind speed (Chirizzi et al., 2021; Coccia, 2020c; Srivastava, 2021). People are dependent on supermarkets, postal, hospitals and banking services for their daily needs and access to these cannot be obstructed, even during lockdowns. Since, the spread is still growing, it is befitting to say that physical or social distancing is not a strong enough preventative measure to avoid infection (Cooper, 2020; Goel et al., 2020b; Singh and Adhikari, 2020). Technological solutions can help to avoid human contact with surfaces in public places (e.g., door handles, elevator buttons) by implementing voice recognition, facial recognition, the sensor for detection of the human presence, etc. However, limiting the airborne spread is complicated, especially in indoor conditions and single air exchange systems (e.g., cruise ships, public buildings, etc.). A study recently suggested that using a surgical mask could be an effective strategy against the spread of COVID-19 (Leung et al., 2020), however, even a mask cannot guarantee that a microdroplet would not be released from its edges. New research suggests that these masks have not been tested for peak exhalation speeds for a coughing and sneezing person (Bourouiba, 2020) thus it is unknown whether these masks are safe or not for containment of SARS-CoV-2. It further leads to the question, whether the use of masks should be mandatory in all public places. The results of recent research also raised the question on the currently accepted social distancing norm of 6 feet as authors have found that micro droplets can carry SARS-CoV-2 virus up to 27 feet (Bourouiba, 2020). Under the current situation, built-up spaces with small rooms and single air exchange systems require proper air filters. The World Health Organization (WHO) Laboratory Biosafety Manual (3rd edition) requires Biosafety Level 2 (BSL-2) requirements for non-propagative diagnostic laboratories and BSL-3 for laboratories handling high concentrations of live SARS-CoV-2. According to the WHO biosafety guidance for SARS-CoV-2, the exhaust air from a laboratory should be discharged through High-efficiency particulate air (HEPA) filters. It is worth mentioning that particle collection efficiency of a HEPA filter decreases down to about 50 % at particle sizes of 0.5 μm due to diffusion and diffusion-interception regimes of particles with sizes in the range from 0.05 up to 1 μm (DHHS (NIOSH) P, 2003). Therefore, capturing SARS-CoV-2 (\varnothing 60 nm to 160 nm) (Sahin, 2020) is beyond the limits of HEPA filters. Other studies reported bioaerosols as agents of nosocomial viral infections (Bing-Yuan et al., 2018; Stanford et al., 2019). This indicates the need for the design of new air filters to deal with pathogens such as SARS-CoV-2 which was the main motivation of this work.

2.2. State-of-the-art on wet type air scrubbers

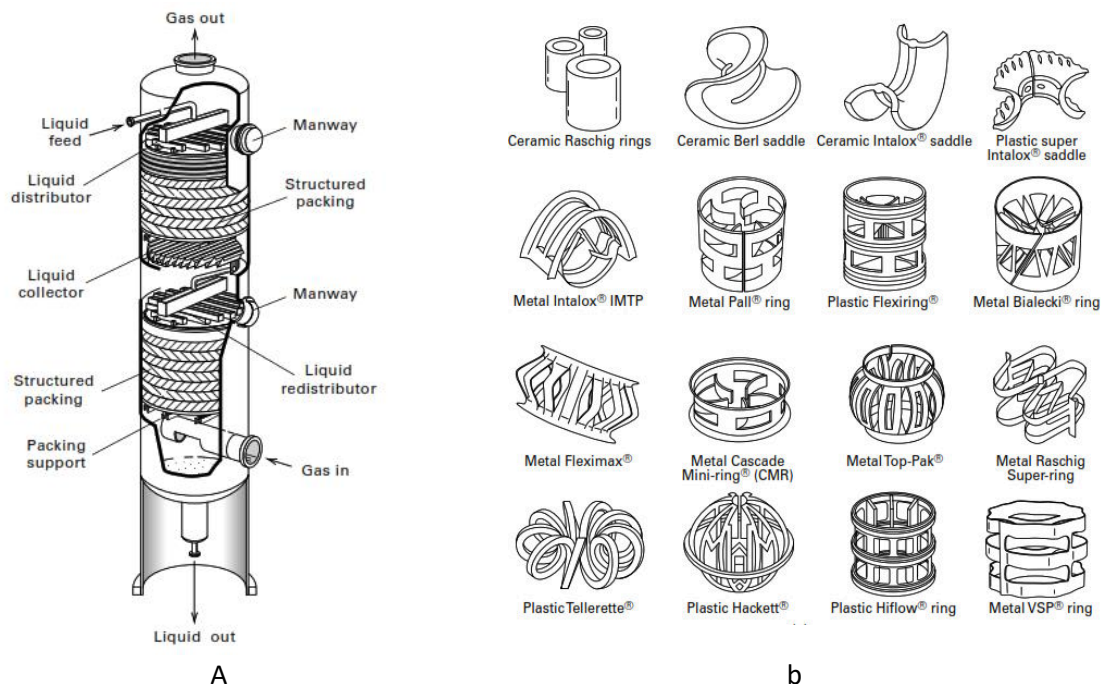


Figure 1. Typical wet type gas scrubber (a) design and (b) typical materials and shape designs used in construction of a packed column (Seader et al., 2011).

The commercially available fabric filters and packed beds, despite having high bioaerosol removal efficiency (Figure 1), require high inactivation efficiency, otherwise incubation of bacteria and viruses may take place (Di Natale et al., 2018; Ghosh et al., 2015; Miaskiewicz-Peska and Lebkowska, 2012; Soret et al., 2018). Negative ion air purifiers (NIAPs) have also been criticised for their adverse health effects (Liu et al., 2020).

Methods to deactivate bioaerosols in the cellular membrane include ultraviolet radiation (Wang et al., 2009), electrostatic precipitation and plasma (Di Natale et al., 2018). However, the incubated bioaerosols collected during filtration can leak through a penetration process during maintenance of the air scrubbing system (e.g., leakage during removal of packing material) (Lee et al., 2007; Miaskiewicz-Peska and Lebkowska, 2012). Therefore, such existing scrubber designs are required to maintain a high degree of disinfection inside the scrubber for the entire operational period. Table 1 summarises the previous work done for the removal of bioaerosols in air filtration. It may be noticed that the previous approaches have used non-recyclable material such as polypropylene, polyacrylonitrile, etc. along with silver particles and thyme oil as antimicrobial agents. Previous approaches were detrimental to the environment (non-cleaner) as the use of nanoparticles is questionable and the antimicrobial agents are very costly. These antimicrobial filters may be suitable only for a short duration of time as the dust accumulated over time will render them ineffective (Ghosh et al., 2015).

Table 1: Previous work on development of antimicrobial air filter

| S. N. | Filter material | Anti-microbial protection | Filtration efficiency | Reference |
|-------|---|---|---|----------------------------|
| 1. | Non-electrostatic melt-blown polypropylene filters | AgNPs/NSP solution over filter material | Antimicrobial efficiency of AgNPs/NSP modified filter of 63 ppm for E. coli was 95.1% at RH of 30%. Antimicrobial efficiency for <i>Candida famata</i> was 91% at RH of 70%. | (Chen et al., 2016) |
| 2. | Fixed bed reactor packed with AgZ | Antibacterial Ag-zeolite (AgZ) | Antibacterial efficiencies of 1, 2 and 3 wt% AgZ against bacterium and the fungus were higher than 95% after 120 minutes of operation, and 1 wt% AgZ was more cost-effective since its antibacterial efficiency approaches 90% in less than 60 min. The 1 wt% AgZ showed excellent performance during repeated usage up to nine times. | (Cheng et al., 2012) |
| 3. | Fibrous air filter media Four types of fibrous air filter media (A, B, C, and D) based on EN779 and EN1882. Types A and B are medium efficiency filter media to remove all particles more than 1 µm, while Type C and D are HEPA media to remove small particles more than 0.3 µm. | None | Efficiency of the filtration on E. coli bioaerosol was lower than that of S. marcescens. The reason for this may be the errors in counting the E. coli colonies when background environmental microorganisms from the air have the same colony appearances. Medium efficiency air filters are suitable for filtering biological particles in air-handling units. The filter efficiency measured with dioctyl phthalate particles of 1 µm was found useful for predicting the removal efficiency of bioaerosols for the filter medium. | (Liu et al., 2009) |
| 4. | Polyacrylonitrile fibres were spun on a substrate by centrifugal spinning | Thyme essential oil | Reductions in bacterial count of <i>Escherichia coli</i> and <i>Staphylococcus aureus</i> with efficiency of 99.99% | (Salussoglia et al., 2020) |
| 5. | Dielectric barrier discharge plasma source was used to directly inactivate suitably produced bioaerosols containing <i>Staphylococcus epidermidis</i> or | None | CAP can induce a log R around 3.76 on bacterial bioaerosol and degrade viral RNA in a short residence time (<0.2 s) | (Bisag et al., 2020) |

| | | | | |
|----|---|--|---|--------------------------|
| | purified SARS-CoV-2 RNA flowing through it. | | | |
| 6. | Wet electrostatic scrubbing. Two configurations were explored: CDES (Charged Droplet Electrified Scrubber) and OPES (Opposite Polarity Electrified Scrubber). | None | Tests were performed with <i>Staphylococcus epidermidis</i> . When operated with charged droplets, the removal efficiency was > 90% by operating with a liquid-to-gas ratio of 2.4 L m ⁻³ gas. The opposite polarity efficiency was > 99% for the liquid-to-gas ratio > 0.8 L m ⁻³ gas. | (Di Natale et al., 2018) |
| 7. | Self-cleaning filter comprised of laser-induced graphene (LIG), a porous conductive graphene foam | None | Periodic Joule-heating mechanism, the filter readily reaches >300 °C. This destroys any microorganisms including bacteria, allergens, exotoxins, endotoxins, mycotoxins, nucleic acids, and prions. | (Stanford et al., 2019) |
| 8. | Medium air filter | Silver nanoparticles approximately 11 nm in diameter | Anti-viral quality factor decreased with increasing dust load but increased with increasing coating areal density. | (Joe et al., 2016) |

Gas-liquid separation or gas absorption by liquid are typical approaches in existing wet scrubbers mainly operating in counter-flow scrubbing mode. Such scrubbers are commonly designed with many packing materials to increase liquid-gas contact area. Large variations of aqueous and non-aqueous air disinfection substances are available for dispersion either as an aerosol or vapour at enough concentration in the path of contaminated air streams.

However, such a scrubber design requires complicated shape packing materials to provide functionality and proper operability. These packing materials are commonly produced from metals, polymers and relatively dense ceramics. Despite the low toxicity of the commonly applied chemical substances (e.g., propylene glycol and Triethylene glycol (TEG)), the negative effect on living organisms (human and animals) and environmental pollution becomes an issue at high consumption rates.

The widely used oxidising agents such as H₂O₂ decompose to form water and oxygen. The vapor of H₂O₂ has been deemed hazardous to the respiratory system and eyes. The permissible exposure limit is 1 ppm according to the Occupational Safety and Health Administration standard 1910.1000 TABLE Z-1. The concentration of 75 ppm is regarded as dangerous to health according to the National Institute for Occupational Safety and Health in their published table of Immediately-Dangerous-To-Life-or-Health values. Therefore, active gas flow disinfection performance in wet scrubbers with H₂O₂ requires not only the highest possible contact area between liquid and gas but also the highest

efficiency of H_2O_2 *in-situ* decomposition arising from the gas-liquid interface. The decomposition of H_2O_2 should be efficient enough to reduce the remaining concentration of H_2O_2 in the cleaned air stream down to 1 ppm or less. The scrubber packing material therefore should exhibit not only a relatively large surface area, but also provide the catalytic H_2O_2 decomposition initiator at the same time. The scrubber construction should be designed to be robust and reliable to avoid the appearance of high H_2O_2 concentration in the air stream, even during catastrophic failure in material or operational mode of the reactor for safe use in public places. Proposed clay-glass porous ceramic materials naturally saturated by Fe_2O_3 provides the required catalytic properties.

2.3. Brief review of various materials proposed for designing new wet scrubber

2.3.1. Clay-ceramic foam with open structure

Clay is one of the most widespread natural materials and readily available resources. Production of tailored and hierarchically structured highly-porous clay ceramic is challenging due to the requirement of high temperatures (up to 1200 °C), leading to enriching closed pore structures and low-surface area (Colombo et al., 2010). Different approaches have been reported on the production of porous clay ceramic materials with high gas and liquid-permeable porosity. For example, Shishkin et.al. (2015) used glass cullet for production of an open cell structure made of clay ceramic with highly open porosity (up to 79 %) and mechanical durability obtained at relatively low sintering temperatures – below the clay self-expanding temperature. Such approaches (direct foaming) lead to interconnected pore structures enabling the possible use of clay ceramics for filtration. The addition of milled glass in the range of 5 to 10 wt. % facilitate mechanical strength at lower (800-950 °C) firing temperatures (Shishkin et al., 2020b). Another, clay-based porous material – clay ceramic hollow spheres were also investigated (Shishkin et al., 2016). They were obtained from red clay containing high Fe_2O_3 , fired at 950 °C and achieved a specific surface area of $1.9 \text{ m}^2 \cdot \text{g}^{-1}$.

Clay ceramic foams (CCF) exhibit the formation of natural-hierarchically structured porous structures (Lakshmi et al., 2015; Zhou et al., 2018). Typical interconnected pore structures of the highly porous ceramics are demonstrated in Figure 2. (Kroll et al., 2014) demonstrated the possibility of obtaining a tailored porous structure by controlling ceramic slurry stirring intensity during direct foaming, as shown in Figure 2. In all cases, struts were observed to be highly porous, especially in Figure 2(b).

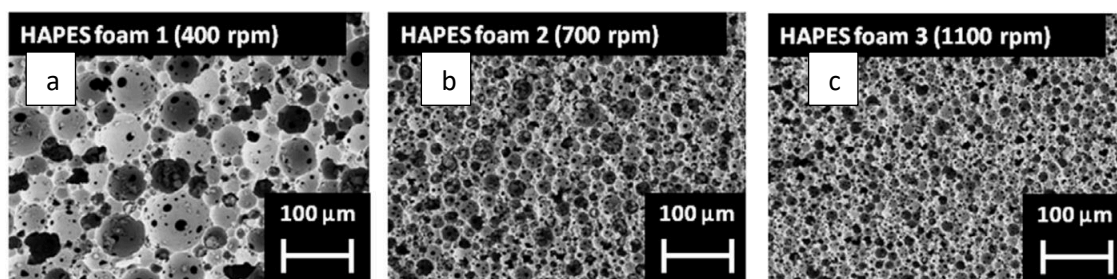


Figure 2. The dependence of the highly porous alumina ceramic foam microstructures and pore size distributions on the applied rotational speed during direct foaming process: a) 400 RPM b) 700 RPM and c) 1100 RPM (Kroll et al., 2014).

2.3.2. *The role of iron oxide as a catalyst in the decomposition of H₂O₂ into free radical oxygen inside porous ceramic*

In 1894, (Fenton, 1894) discovered a process to generate strong oxidants through a reaction between Fe(II) and H₂O₂. He proposed using Fenton-like reagents such as Fe (III)/H₂O₂, photo-/electro- combinations to achieve industrial scale oxidation. This approach has since been utilised in multiple applications across various fields including the cognition of biological stress response (Liu et al., 2004; Wardman and Candeias, 1996).

The readily available red illite clay is known to have high content of iron oxide (Fe₂O₃ and Fe₃O₄) which makes it a useful catalyst for decomposing hydrogen peroxide (Koppenol and Hider, 2019; Wang et al., 2015; Wu et al., 2019) shown by equation (1):



The detailed reaction mechanism depends on various factors such as pH, aqueous or organic solvent (Koppenol and Hider, 2019; Wang et al., 2015; Wardman and Candeias, 1996). An understanding on this topic is still being further developed (Filipovic and Koppenol, 2019). Both Hematite (Fe₂O₃) and Magnetite (Fe₃O₄) could be present in the clay. Hence, the overall reactions could be described as Fenton chemistry. Ferrous can oxidize to ferric in the presence of H₂O₂ and ferric could be reduced to ferrous as depicted in equation (2) and (3).



The Fenton reaction efficiently eliminates the structure of recalcitrant organic pollutants at near diffusion-controlled rates based on the generation of strong, relatively non-selective hydroxyl radicals HO• and hydroperoxyl radicals HO₂• (Garcia-Segura et al., 2012; Lucas et al., 2007; Wardman and Candeias, 1996). Hydroperoxyl radical HO₂• is conjugate acid of superoxide as shown in equation (4) (Wardman and Candeias, 1996).



Active gas flow disinfection efficiency will be at its best when having the maximum possible contact area between the liquid and gas. It will also result in decomposition of H₂O₂ caused by the collisions between gas and liquid particles. Accordingly, we propose that the filter intended to deactivate microbes should not only possess a relatively large surface area but will also provide the catalyst for H₂O₂ decomposition at the same time. The proposed clay-glass porous ceramic material naturally saturated by Fe₂O₃ provides the required catalytic properties and offers the potential use of virucidal agent, thus tackling the problem of indoor spread of SARS CoV-2.

One of the most important requirements in the design of filter is the uniform distribution of the H₂O₂ decomposing catalyst (Fe₂O₃) in the whole volume of the highly porous clay ceramic filter. To this end, it is proposed to use highly porous clay-glass open-cell foam as an easily reproducible and cheap air filtering and disinfection material. The in-situ decomposition of H₂O₂ is highly effective in disinfection of air stream by highly reactive atomized oxygen. The nature of mostly oxidized crystalline phases in glass-clay ceramic exhibits high stability to chemical oxidation caused by atomized oxygen. Such an approach results in filtered air with relatively high moisture content and a low content of biologically hazardous contaminants.

It is worth mentioning that beside clay, it is also possible to use any ceramic foam production method and materials. However, such an approach requires three key factors: 1) interconnected pore structure; 2) high porosity of pore struts and 3) uniform distribution of catalyst throughout the volume of ceramic foam. For example, it is possible to use kaolinite or bentonite-type clay foams with a very low Fe₂O₃ content or Al₂O₃ (Svinka et al., 2011; Zake-Tiluga et al., 2014), SiO₂ (Binks, 2002), cordierite (Song et al., 2006), mullite (Zake-Tiluga et al., 2015) or other foams (Colombo and Scheffler, 2005); however, during production, these materials will need to saturate with catalysts such as magnesium oxide (MnO) or Fe₂O₃.

3. Materials and methods

3.1 Production of clay ceramic foam (CCF)

Homogenized clay collected from Liepa’s clay deposit (*Lode LTD*, Liepa Latvia) and green bottle glass were used for the clay ceramic foam (CCF) production. More details about the production of CCF are available from elsewhere (Shishkin et al., 2020b), however, specific details of the procedure are provided here for the purpose of brevity. The laboratory scaled high speed rotary disintegrator DSL-175 was used for the preparation of clay and clay-glass powders with glass concentrations of 0, 5, 7 and 10 wt. %. High speed mixer disperser (HSMD) with cavitation effect was used for the preparation of aqueous clay and clay-glass suspensions and subsequent direct foaming. The HSMD was set at a rotational speed of 500 rpm and the system was set in circulation mode. The system was filled with 300 ml of water and 1 wt. % (calculated from dry clay or clay-glass mixture with the total added weight of 6.5 g) of dispersant was subsequently added. The clay-glass powder (700 g) was added to the circulating system with the relatively low feed rate of ~300 g·min⁻¹ with the purpose of avoiding agglomeration; the rotational speed of the HSMD was gradually increased up to 4000 rpm. The foaming agent with the concentration of 5.5 wt. % (calculated according to total weight of dry clay or clay-glass powder – 38.5 g) was added over 30 seconds; the rotational speed of the HSMD was gradually increased up to 6000 rpm. The air supply valve was opened and held until the volume of the suspension increased two-fold. The foamed suspension obtained was recirculated in the HSMD system for 1 min. The specimen designations and slurry compositions tried and tested are shown in Table 2 where WG-mean waste glass, first one-digit number means glass content in wt.% and remaining three-digit number means firing temperature.

Table 2: Specimens designation and slurry composition

| Specimen | Firing temperature, °C | Clay, g | Glass, g | Glass content, % | Water, ml | Foaming agent, ml | Electrolyte, g |
|----------|------------------------|---------|----------|------------------|-----------|-------------------|----------------|
| WG0-950 | 950 | 700 | 0 | 0 | 300 | 38.5 | 6.5 |
| WG5-800 | 800 | 665 | 35 | 5 | | | |
| WG5-850 | 850 | | | | | | |
| WG5-900 | 900 | | | | | | |
| WG7-950 | 950 | | | | | | |
| WG7-800 | 800 | 649 | 51 | 7 | | | |
| WG7-850 | 850 | | | | | | |
| WG7-900 | 900 | | | | | | |
| WG7-950 | 950 | | | | | | |
| WG10-800 | 800 | 630 | 70 | 10 | | | |
| WG10-850 | 850 | | | | | | |
| WG10-900 | 900 | | | | | | |
| WG10-950 | 950 | | | | | | |

The foam suspension was thence filled into moulds of internal dimensions 150×150×60 mm and subsequently dried in the air for 72 h at room temperature. Corrugated cardboard was used in fabrication of moulds to provide uniform water evaporation from foamed suspension. Naturally dried specimens were dried in a furnace at 105 °C while retaining the mass. The selected duration of the drying was 24 h. Dried samples were removed from moulds and subsequently cut into specimens with dimensions 55×55×110 mm. The specimens were thermally sintered in the muffle furnace (LH11, P330 by Nabertherm) at selected temperatures 800 °C, 850 °C, 900 °C and 950 °C under oxidising atmosphere (air). The heating rate was kept at 5 °C·min⁻¹. The duration of sintering at selected temperature was kept as 30 min. Sintered specimens were finally cooled down to room temperature. Sintered foamed ceramic samples were cut and polished down to a final size of 50×50×50 mm.

3.2 Physical and Mechanical Properties

Thermal sintering shrinkage of foamed ceramic samples was measured with help of a calliper. The pycnometer and the Archimedes method (*Annual book of ASTM standards, ASTM Standards C20*, 2010) were applied for determination of the apparent density, bulk density and apparent porosity and water absorption capacity. The sum of open and closed porosities was used for calculation of the apparent density. Compressive strength of the sintered samples with dimensions of 25×25×25 mm was measured with the help of a Universal Testing Machine (UTM, Instron 8801, Germany) according to the testing standard ASTM D695. Every test was repeated 6 times and the average values and standard deviations were calculated. The optical microscope VHX-2000 (Keyence Corporation, Osaka, Japan) equipped with VH-Z20R/W lens was used for characterisation of surface morphology and microstructure of fractured foamed ceramic samples. A scanning electron microscope (SEM) Zeiss EVO MA-15 (Carl Zeiss AG, Oberkochen, Germany) was used for microstructural characterization of pore structures and pore walls. Optical dilatometry was performed with the help of the high temperature optical microscope EM201 HT163

(Hesse instruments, Germany). Specific surface area of samples was determined according to the Brunauer, Emmett and Teller (BET) theory with the help of QUADRASORB SI Kr/ (Quantachrome, USA) equipped with Standard Autosorb degasser at 300 °C.

4. Results and Discussions

4.1 Surface morphology and physio-mechanical properties

An intensive shrinkage and fracture of foamed clay was observed during the drying process shown in Figure 3. The addition of coarser glass particles avoided cracking during drying and thermal sintering of the foamed clay suspension at lower temperature. The dimensions of moulded glass containing ceramic foams also remain relatively unchanged after drying and thermal sintering processes, which may be seen from Figure 3 (b) and 3(c). The size of pores generated with the help of the direct foaming process were in the range of 50 μm to 250 μm with uniform distribution in foamed clay ceramic materials, as shown in the SEM images (see Figure 4).

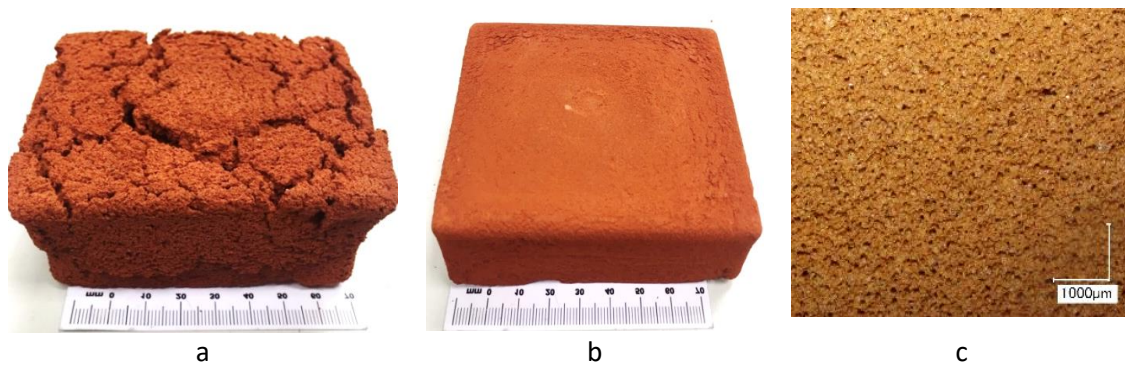


Figure 3. Foamed clay ceramic samples after sintering at 950 °C: a) WG0-950 (without glass); b) WG10-950 (with glass) – general view of the sample and; c) WG10-950 optical microscopy image (30x magnification).

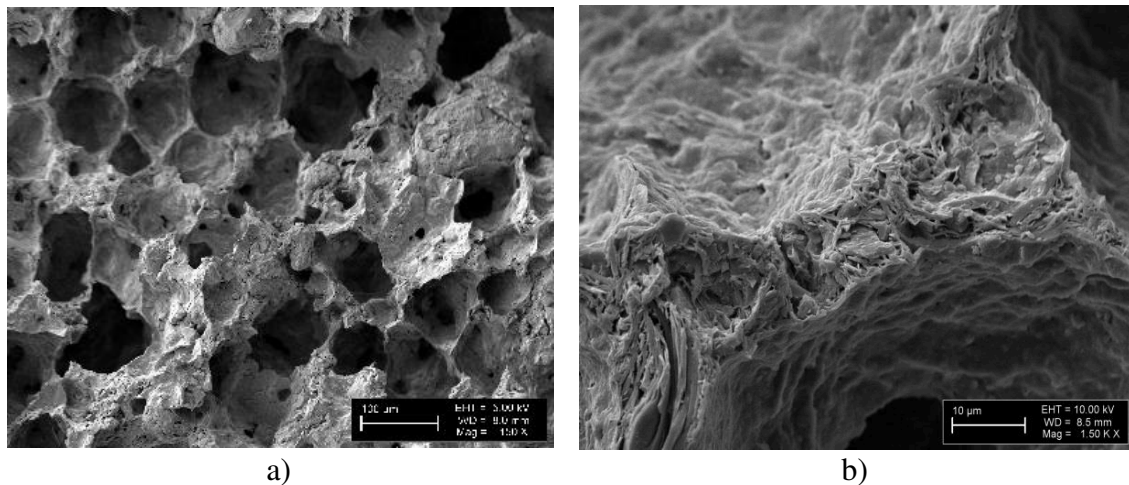


Figure 4. SEM images of fractured foamed clay ceramic sample WG5-950: a) general pore structure (100x magnification) and; b) structure of the pore wall (1500x magnification) (Shishkin et al., 2020a).

The release of mechanically bonded water, combustion of organic matter and decomposition of carbonaceous materials lead to the formation of pores with sizes under 1 μm , as demonstrated in Figure 4 (b). Also, an increase in the sintering temperature from 800 up to 950 $^{\circ}\text{C}$ leads to the decrease of the pore size (Figure 5) as well as a dramatic decrease in specific surface area (Figure 6) from (15-18) $\text{m}^2\cdot\text{g}^{-1}$ up to (0.6-0.8) $\text{m}^2\cdot\text{g}^{-1}$.

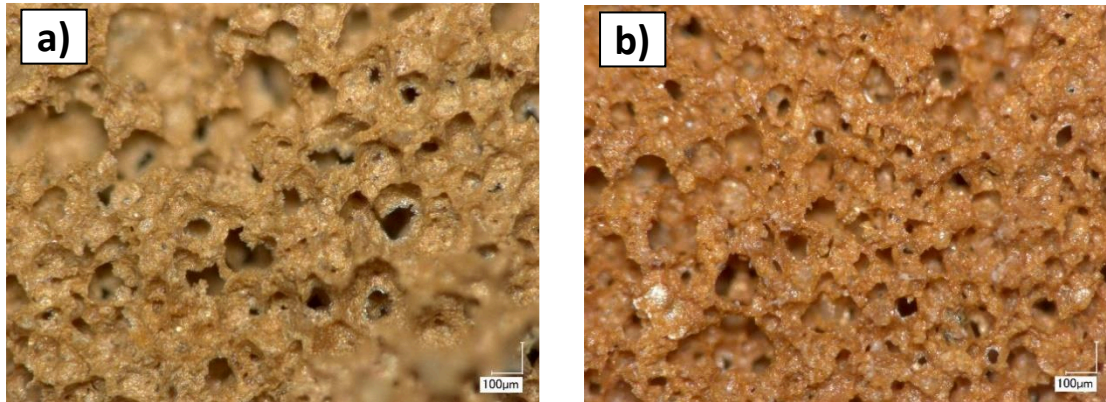


Figure 5. The optical microscopy images of glass containing foamed clay ceramic materials cross section: a) WG5-800 $^{\circ}\text{C}$; b) WG5-950 $^{\circ}\text{C}$.

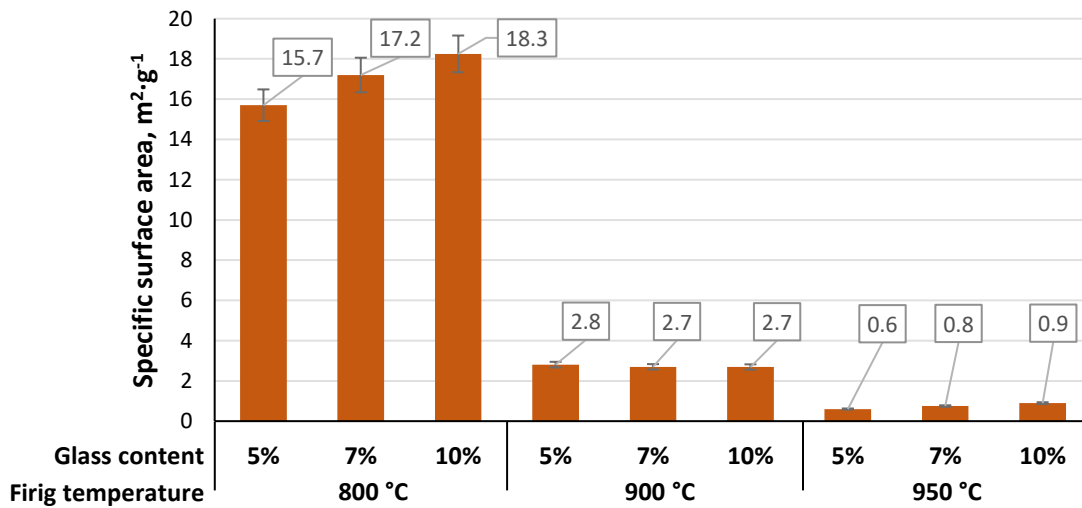


Figure 6: Influence of the glass-cullet loading (5, 7 and 10 wt. %) and firing temperature on the highly porous clay ceramic surface area (acquired using N_2 BET)

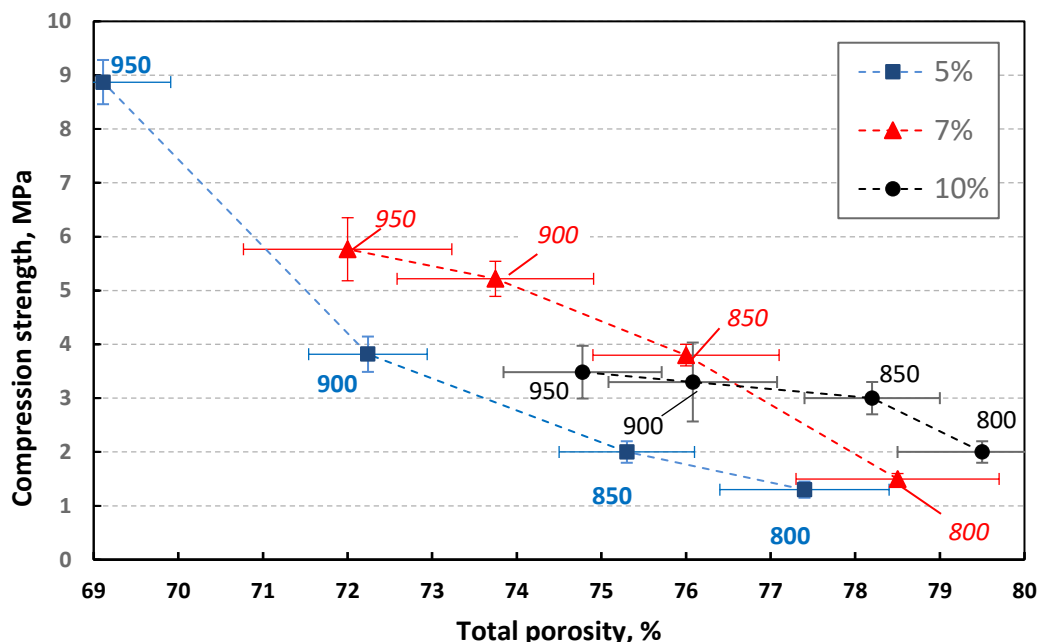


Figure 7: Influence of the glass-cullet loading (5, 7 and 10 wt. %) and firing temperature on the compression strength and total porosity. MC loading is indicated in the legend. The thermal sintering temperatures are indicated in °C (Shishkin et al., 2020a).

The dependence of total porosity and compressive strength on the glass-cullet loading (5, 7 and 10 wt. %) and thermal sintering temperature is shown in Figure 7. Results evidently suggest that the increase in the glass-cullet concentration leads to decreased compression strength and increased total porosity of sintered materials. The utilisation of the glass-cullet increases the total porosity of the CCF up to 78-79.5 % at the lowest selected sintering temperature, indicating the selected glass as the melting agent in clay ceramic material.

Our design calculations revealed that the CCF with compressive strength of 1.5 to 2.0 MPa for WG7-800 and WG10-800 specimens is sufficient to carry air-pressure load for the proposed novel design of air filters. Relatively high (up to $18 \text{ m}^2 \cdot \text{g}^{-1}$) specific surface area (Figure 6), is crucial for ceramic filters with catalytic reaction for H_2O_2 decomposition. Such partially open-cell structure in combination with relatively high and uniformly distributed Fe_2O_3 will be an ideal candidate for production of simple, inexpensive wet scrubber-reactor with operational principle based on the H_2O_2 catalytic decomposition.

4.2. Air filter design using clay ceramic foams (CCF)

The newly designed reactor makes use of the widely available natural recycled materials clay and glass cullet. Overall, the design rationale was based on the footings of achieving two sustainability development goals (i.e., SDG 3 and SDG 15) aiming to provide cleaner natural resources (air, water and land) for healthy living, thus avoiding a recurrent spread of a pandemic problem such as COVID-19. Various examples drawn from the previous literature have indicated the use of non-recyclable material such as polypropylene, polyacrylonitrile, etc. along with silver particles, thyme oil as antimicrobial agents in

developing the air filters. These materials are produced using non-cleaner methods of production and are therefore not sustainable. Moreover, the antimicrobial filters made from these materials are unsuitable for long-lasting performance since the dust accumulated over time renders them ineffective.

Based on the aforementioned discussions and results, a proposed design rationale of the single filtration unit is demonstrated in Figure 8. The main parts of the setup shown in Figure 8(a) are:

- (1) the reservoir for supply of H_2O_2 ;
- (2) porous ceramic filter; and
- (3) the reservoir with opening for the collection or transfer of the remaining H_2O_2 into the next reservoir.

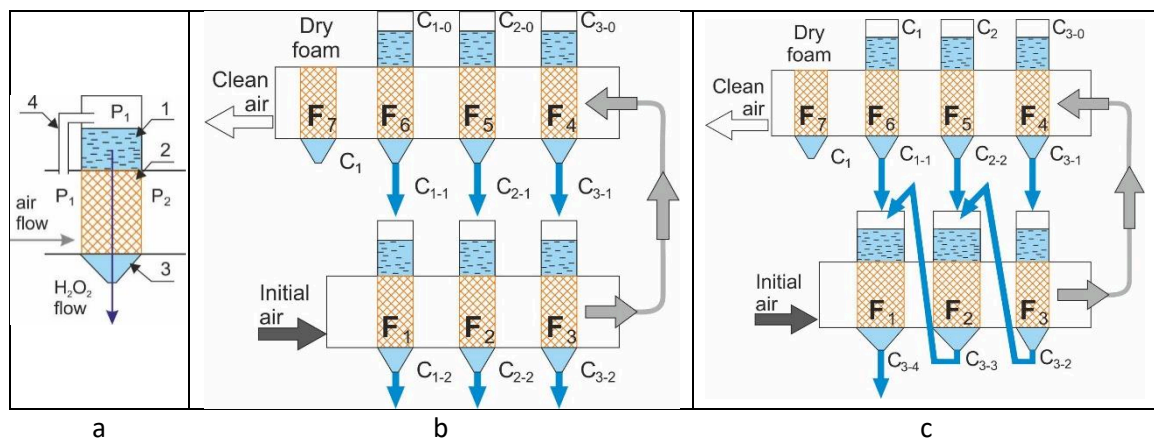


Figure 8. Principle scheme of the air filtration system: a) filter unit scheme consisting of 1 - reservoir for H_2O_2 supply, 2 - ceramic filter, 3 – reservoir with the opening for collection and transfer of the remaining H_2O_2 , 4- bypass for pressure alignment, P_1 and P_2 – air pressure before and after ceramic filter; and filtering setups with H_2O_2 b) “direct flow” and c) “continuous counterflow” modes.

The flow directions of the supplied air and H_2O_2 solution are generally oriented orthogonally to each other. The natural airflow resistance of the ceramic filter saturated with H_2O_2 solution causes pressure drop ($P_1 > P_2$) by preventing air leak into the reservoir (1). The continuity in H_2O_2 solution flow is provided with the bypass for pressure alignment (4).

Two possible options for filtering unit layouts and H_2O_2 solution flows are presented in Figure 8(b) and (c). The initial concentrations of applied fresh H_2O_2 solution are: $C_{3-0} > C_{2-0} > C_{1-0}$; remaining H_2O_2 concentrations after first cycle are: $C_{3-1} > C_{2-1} > C_{1-1}$; and C_{3-3} and C_{3-4} are remaining H_2O_2 concentrations after third and fourth cycles, respectively. The example of initial concentrations of H_2O_2 in solutions could be 5-7 % (C_{1-0}), 15-10 % (C_{2-0}), and 15-20 % (C_{3-0}). Concentrations of H_2O_2 increases gradually in the solution until reaching maximum designed concentration in filtration unit F_4 and subsequently decreases in units F_5 and F_6 with the aim of capturing H_2O_2 solution droplets with highest concentrations from F_3 and F_4 , as demonstrated for both designs in Figure 8(b) and (c). The dry foam F_7 is aimed at capturing residual droplets and avoiding possible solution leaching from the last filtration unit. The combination of sequential counter-flow (from F_3 to F_2 and

F₂ to F₁) and cross-units flow (from F₅ to F₂ and F₆ to F₁) is demonstrated in the Figure 8(c). In this case H₂O₂ solution flow rate increased from unit F₃ to F₂ and from F₂ to F₁ due to the increased H₂O₂ feed rate from units F₅ and F₆.

Such an approach could be beneficial due to a decreased pressure drop by providing higher air flow rate (higher permeability) in ceramic foam with larger pores which results in more efficient gravity assisted H₂O₂ solution flow. Any unused H₂O₂ solution (C₁₋₁, C₂₋₁, C₃₋₁, and C₃₋₄) can be utilised for disinfection of indoor and outdoor surfaces by considering all safety issues.

The actual mechanism of the filtration will become clearer through modelling informed experiments which we will expand in our follow-on work. However, based on the design proposed in figure 8, the most plausible mechanism which will govern the filtration and disinfection is depicted in Figure 9 (a, b and c).

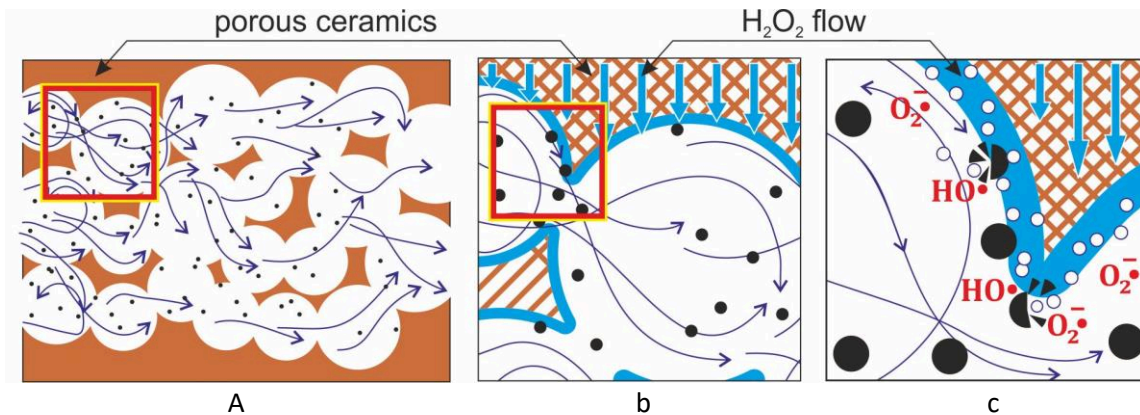


Figure 9. The contaminated gas motion in porous structure (a) acceleration and collisions of particles during passing narrow openings of interconnected pores (b) causing increased number of collisions and (c) destructive reactions between contaminants and active radicals (HO•, O₂^{•-} are hydroxyl and superoxide radicals described in equation (1) to (4)).

The direction vector of the initially supplied contaminated air changes from laminar to turbulent during entrance to the porous ceramic structure (Figure 9 a). The passage provided by the pore connection windows, where cross section is much smaller than pore diameter causes an increase in the linear speed of the flow. Turbulent motion of the air leads to increased number of viral particle collisions with pore walls saturated with the H₂O₂ solution (Figure 9 b and c). Turbulent motion also leads to mechanical trapping of particles in the porous pore struts (mechanical filtering mechanism). The velocity of air and contaminant particles increases during movement through channels between interconnected pores with smaller diameters. Perpendicularly oriented H₂O₂ solution streams penetrate through the porous structure and wet internal walls of pores. The presence of Fe₂O₃ or other catalyst causes formation of the atomized oxygen from supplied H₂O₂ which was demonstrated by equations (1) and (2). Contaminants from the air stream collide and react with atomized oxygen leading to neutralization (e.g., deactivation of the microbes).

5. Conclusions

Indoor environments especially in malls, gyms, hospitals and religious places can accelerate the spread of infectious diseases and one way of controlling it is by continuous disinfection of air to make breathing air free from pathogens. An air filter can significantly improve hygiene and reduce the cause of the spread of pathogens. While personal control measures like wearing a face mask are necessary, engineering control measures (i.e., air filter) are equally important. Inspired by the immediate and urgent need to de-risk the indoor spread of coronavirus (one of the recently identified pathogens), this work proposes a circular economy driven design-led effort to guide the fabrication of a novel wet scrubber-reactor. The filter will benefit the development of an air-filtration system to deactivate airborne pathogens (bioaerosols). Following specific outcomes were made from this study:

1. Fenton’s theory can be used to recycle indoor air using the principles of the circular economy. This work shows that the readily available red illite clay material which has a rich presence of iron oxide can be used to decompose hydrogen peroxide (H_2O_2) to generate fresh oxygen. H_2O_2 has been approved by the FDA in the US for disinfecting respiratory filters from coronavirus. This design uniquely implements the collision mode between perpendicularly oriented gas molecules and H_2O_2 solution inside of an open-cell structured highly porous ceramic foam.
2. It has been shown that the cellular structure in an open foam leads to generate turbulent airflow and the narrow opening between the interconnected pores increases the velocity and number of desired collisions between contaminating particles and porous pore struts. The proposed filter unlike the currently available commercial filter can avoid the problem of plugging and will have a longer lifespan.

Overall, it was concluded that the high air filtration and disinfection efficiency possible to be achieved from the proposed design are facilitated by the: i) uniform distribution of iron oxide in the red illite clay ceramics catalysing the formation of atomized oxygen from supplied H_2O_2 ; ii) hierarchically structured porous low-temperature sintered clay-glass ceramic material providing high contact area between atomized oxygen and supplied air with biohazardous contamination; iii) the column type design solution makes the proposed setup easily deployable for readily preparing any such future issue for tackling bio-hazard challenges. Proactive measures such as this are immensely required in the current scenario considering the threat posed by the pandemics. Also, taking the circular economy route in developing engineering solutions helps achieve sustainability development goals. Much like the other scientific studies, this study has raised some open questions which will be answered through a follow-on study and these include questions such as (a) determining health effects to individuals with long-term exposure to hydrogen peroxide radicals; (b) effects on the level of air pollution; (c) effect of meteorological factors on the performance of proposed filter (d) ideal location of the filter in the space and (e) establishing filtration rate. Overall, it can be concluded that the development of an air filter meeting the goal of sustainable development while aiding the needs of environmental, energy, economy, and acoustic comfort can be treated as a policy matter in the societal interest.

Acknowledgements

The authors would like to thank Faculty of Materials Science and Applied Chemistry, Riga Technical University for providing the facilities. We express thanks to the STSM support from Cost Action CA17133 (funded by H2020) to enable the UK-Latvian collaboration. SG is particularly thankful to the Royal Academy of Engineering, UK to sponsor GG through the Indo-UK partnership Industry-academia and Engineering-X Pandemic Preparedness award (Grant No. IAPP18-19\295 and EXPP2021\1\277).

SG would also like to acknowledge the financial support provided by the UKRI via Grants No.: EP/L016567/1, EP/S013652/1, EP/S036180/1, EP/T001100/1 and EP/T024607/1, Royal Academy of Engineering via Grant No. TSP1332, EU Cost Actions CA18125, CA18224 and CA16235 and Royal Society’s Newton Fellowship award NIF\R1\191571. We are also thankful to European Regional Development Funds (ERDF) sponsored A2i project at LSBU that has catalysed several industrial partnerships. Wherever applicable, the work made use of Isambard and ARCHER2 high-performance computing resources based in the UK accessed via Resource Allocation Panel (RAP) grant as well as the EPSRC project.

Research Data statement

Data underlying this paper can be accessed from Cranfield repository:

10.17862/cranfield.rd.13708369

References:

- Andersen, K.G., Rambaut, A., Lipkin, W.I., Holmes, E.C., Garry, R.F., 2020. The proximal origin of SARS-CoV-2. *Nat. Med.* <https://doi.org/10.1038/s41591-020-0820-9>
- Annual book of ASTM standards, ASTM Standards C20, 2010. , Standard Test Methods for Apparent Porosity, Water Absorption, Apparent Specific Gravity, and Bulk Density of Burned Refractory Brick and Shapes by Boiling Water.
- Belosi, F., Conte, M., Gianelle, V., Santachiara, G., Contini, D., 2021. On the concentration of SARS-CoV-2 in outdoor air and the interaction with pre-existing atmospheric particles. *Environ. Res.* 193, 110603. <https://doi.org/10.1016/j.envres.2020.110603>
- Bing-Yuan, Zhang, Y.-H., Leung, N.H.L., Cowling, B.J., Yang, Z.-F., 2018. Role of viral bioaerosols in nosocomial infections and measures for prevention and control. *J. Aerosol Sci.* 117, 200–211. <https://doi.org/10.1016/j.jaerosci.2017.11.011>
- Binks, B.P., 2002. Macroporous Silica From Solid-Stabilized Emulsion Templates. *Adv. Mater.* 14, 1824–1827. <https://doi.org/10.1002/adma.200290010>
- Bisag, A., Isabelli, P., Laurita, R., Bucci, C., Capelli, F., Dirani, G., Gherardi, M., Laghi, G., Paglianti, A., Sambri, V., Colombo, V., 2020. Cold atmospheric plasma inactivation of aerosolized microdroplets containing bacteria and purified SARS-CoV-2 RNA to contrast airborne indoor transmission. *Plasma Process. Polym.* 17, 2000154. <https://doi.org/10.1002/ppap.202000154>
- Bourouiba, L., 2020. Turbulent Gas Clouds and Respiratory Pathogen Emissions. *JAMA.* <https://doi.org/10.1001/jama.2020.4756>

- CDC, 2020. How Coronavirus Spreads [WWW Document]. Natl. Cent. Immun. Respir. Dis. (NCIRD), Div. Viral Dis. URL <https://www.cdc.gov/coronavirus/2019-ncov/prevent-getting-sick/how-covid-spreads.html> (accessed 3.29.20).
- Chen, J.-W., Lee, G.W.-M., Chen, K.-J., Yang, S.-H., 2016. Control of Bioaerosols in Indoor Environment by Filter Coated with Nanosilicate Platelet Supported Silver Nanohybrid (AgNPs/NSP). *Aerosol Air Qual. Res.* 16, 2198–2207. <https://doi.org/10.4209/aaqr.2016.06.0224>
- Cheng, H.-H., Hsieh, C.-C., Tsai, C.-H., 2012. Antibacterial and Regenerated Characteristics of Ag-zeolite for Removing Bioaerosols in Indoor Environment. *Aerosol Air Qual. Res.* 12, 409–419. <https://doi.org/10.4209/aaqr.2011.08.0134>
- Chirizzi, D., Conte, M., Feltracco, M., Dinoi, A., Gregoris, E., Barbaro, E., La Bella, G., Ciccicarese, G., La Salandra, G., Gambaro, A., Contini, D., 2021. SARS-CoV-2 concentrations and virus-laden aerosol size distributions in outdoor air in north and south of Italy. *Environ. Int.* 146, 106255. <https://doi.org/10.1016/j.envint.2020.106255>
- Coccia, M., 2020a. An index to quantify environmental risk of exposure to future epidemics of the COVID-19 and similar viral agents: Theory and practice. *Environ. Res.* 191, 110155. <https://doi.org/10.1016/j.envres.2020.110155>
- Coccia, M., 2020b. Factors determining the diffusion of COVID-19 and suggested strategy to prevent future accelerated viral infectivity similar to COVID. *Sci. Total Environ.* 729, 138474. <https://doi.org/10.1016/j.scitotenv.2020.138474>
- Coccia, M., 2020c. How do low wind speeds and high levels of air pollution support the spread of COVID-19? *Atmos. Pollut. Res.* <https://doi.org/10.1016/j.apr.2020.10.002>
- Colombo, P., Scheffler, M. (Eds.), 2005. *Cellular Ceramics: Structure, Manufacturing, Properties and Applications, ... Ceramics: Structure WILEY-VCH Verlag, Weinheim.*
- Colombo, P., Vakifahmetoglu, C., Costacurta, S., 2010. Fabrication of ceramic components with hierarchical porosity. *J. Mater. Sci.* 45, 5425–5455. <https://doi.org/10.1007/s10853-010-4708-9>
- Cooper, A., 2020. Coronavirus: why we need to consult engineers as well as scientists for solutions [WWW Document]. *Theconversation.com.* URL <https://theconversation.com/coronavirus-why-we-need-to-consult-engineers-as-well-as-scientists-for-solutions-134460> (accessed 3.29.20).
- DHHS (NIOSH) P, 2003. *Guidance for Filtration and Air-Cleaning Systems to Protect Building Environments from Airborne Chemical, Biological, or Radiological Attacks.*
- Di Natale, F., Manna, L., La Motta, F., Colicchio, R., Scaglione, E., Pagliuca, C., Salvatore, P., 2018. Capture of bacterial bioaerosol with a wet electrostatic scrubber. *J. Electrostat.* 93, 58–68. <https://doi.org/10.1016/j.elstat.2018.04.003>
- FDA, 2020. FDA Issues Second Emergency Use Authorization to Decontaminate N95 Respirators [WWW Document]. URL <https://www.fda.gov/news-events/press-announcements/coronavirus-covid-19-update-fda-issues-second-emergency-use-authorization-decontaminate-n95>
- Fenton, H.J.H., 1894. LXXIII. - Oxidation of tartaric acid in presence of iron. *J. Chem. Soc. Trans.* 65, 899–910. <https://doi.org/10.1039/CT8946500899>
- Filipovic, M.R., Koppenol, W.H., 2019. The Haber-Weiss reaction – The latest revival. *Free Radic. Biol. Med.* 145, 221–222.

- <https://doi.org/10.1016/j.freeradbiomed.2019.09.017>
- Garcia-Segura, S., Garrido, J.A., Rodríguez, R.M., Cabot, P.L., Centellas, F., Arias, C., Brillas, E., 2012. Mineralization of flumequine in acidic medium by electro-Fenton and photoelectro-Fenton processes. *Water Res.* 46, 2067–2076. <https://doi.org/10.1016/j.watres.2012.01.019>
- Ghosh, B., Lal, H., Srivastava, A., 2015. Review of bioaerosols in indoor environment with special reference to sampling, analysis and control mechanisms. *Environ. Int.* 85, 254–272. <https://doi.org/10.1016/j.envint.2015.09.018>
- Goel, S., Hawi, S., Goel, G., Thakur, V.K., Agrawal, A., Hoskins, C., Pearce, O., Hussain, T., Upadhyaya, H.M., Cross, G., Barber, A.H., 2020a. Resilient and agile engineering solutions to address societal challenges such as coronavirus pandemic. *Mater. Today Chem.* 17, 100300. <https://doi.org/10.1016/j.mtchem.2020.100300>
- Goel, S., Knaggs, M., Goel, G., Zhou, X.W., Upadhyaya, H.M., Thakur, V.K., Kumar, V., Bizarri, G., Tiwari, A., Murphy, A., Stukowski, A., Matthews, A., 2020b. Horizons of modern molecular dynamics simulation in digitalized solid freeform fabrication with advanced materials. *Mater. Today Chem.* 18, 100356. <https://doi.org/10.1016/j.mtchem.2020.100356>
- Goldberg, L., Levinsky, Y., Marcus, N., Hoffer, V., Gafner, M., Hadas, S., Kraus, S., Mor, M., Scheuerman, O., 2021. SARS-CoV-2 infection among healthcare workers despite the use of surgical masks and physical distancing - the role of airborne transmission. *Open Forum Infect. Dis.* <https://doi.org/10.1093/ofid/ofab036>
- Greenfieldboyce, N., 2020. WHO Reviews “Available” Evidence On Coronavirus Transmission Through Air [WWW Document]. NPR. URL <https://www.npr.org/2020/03/28/823292062/who-reviews-available-evidence-on-coronavirus-transmission-through-air> (accessed 3.29.20).
- Hassanin, A., 2020. Coronavirus origins: genome analysis suggests two viruses may have combined [WWW Document]. World Econ. Forum. URL <https://www.weforum.org/agenda/2020/03/coronavirus-origins-genome-analysis-covid19-data-science-bats-pangolins/> (accessed 3.29.20).
- Joe, Y.H., Park, D.H., Hwang, J., 2016. Evaluation of Ag nanoparticle coated air filter against aerosolized virus: Anti-viral efficiency with dust loading. *J. Hazard. Mater.* 301, 547–553. <https://doi.org/10.1016/j.jhazmat.2015.09.017>
- Kampf, G., Todt, D., Pfaender, S., Steinmann, E., 2020. Persistence of coronaviruses on inanimate surfaces and their inactivation with biocidal agents. *J. Hosp. Infect.* 104, 246–251. <https://doi.org/10.1016/j.jhin.2020.01.022>
- Koppenol, W.H., Hider, R.H., 2019. Iron and redox cycling. Do’s and don’ts. *Free Radic. Biol. Med.* 133, 3–10. <https://doi.org/10.1016/j.freeradbiomed.2018.09.022>
- Kroll, S., Soltmann, C., Koch, D., Kegler, P., Kunzmann, A., Rezwani, K., 2014. Colored ceramic foams with tailored pore size and surface functionalization used as spawning plates for fish breeding. *Ceram. Int.* 40, 15763–15773. <https://doi.org/10.1016/j.ceramint.2014.07.100>
- Lakshmi, V., Resmi, V.G., Raju, A., Deepa, J.P., Rajan, T.P.D., Pavithran, C., Pai, B.C., 2015. Concentration dependent pore morphological tuning of kaolin clay foams using sodium dodecyl sulfate as foaming agent. *Ceram. Int.* 41, 14263–14269. <https://doi.org/10.1016/j.ceramint.2015.07.056>
- Lee, L.D., Berkheiser, M., Jiang, Y., Hackett, B., Hachem, R.Y., Chemaly, R.F., Raad, I.I.,

2007. Risk of Bioaerosol Contamination With *Aspergillus* Species Before and After Cleaning in Rooms Filtered With High-Efficiency Particulate Air Filters That House Patients With Hematologic Malignancy. *Infect. Control Hosp. Epidemiol.* 28, 1066–1070. <https://doi.org/10.1086/519866>
- Lee, Y.-N., Chen, L.-K., Ma, H.-C., Yang, H.-H., Li, H.-P., Lo, S.-Y., 2005. Thermal aggregation of SARS-CoV membrane protein. *J. Virol. Methods* 129, 152–161. <https://doi.org/10.1016/j.jviromet.2005.05.022>
- Leung, N.H.L., Chu, D.K.W., Shiu, E.Y.C., Chan, K.-H., McDevitt, J.J., Hau, B.J.P., Yen, H.-L., Li, Y., Ip, D.K.M., Peiris, J.S.M., Seto, W.-H., Leung, G.M., Milton, D.K., Cowling, B.J., 2020. Respiratory virus shedding in exhaled breath and efficacy of face masks. *Nat. Med.* <https://doi.org/10.1038/s41591-020-0843-2>
- Liu, G., Xiao, M., Zhang, X., Gal, C., Chen, X., Liu, L., Pan, S., Wu, J., Tang, L., Clements-Croome, D., 2017. A review of air filtration technologies for sustainable and healthy building ventilation. *Sustain. Cities Soc.* 32, 375–396. <https://doi.org/10.1016/j.scs.2017.04.011>
- Liu, J., Qi, R., Li, Q., Han, G., Qi, J., 2009. Filtration of Bioaerosols Using Fibrous Air Filter Media. *HVAC&R Res.* 15, 1165–1174. <https://doi.org/10.1080/10789669.2009.10390884>
- Liu, Q., Berchner-Pfannschmidt, U., Moller, U., Brecht, M., Wotzlaw, C., Acker, H., Jungermann, K., Kietzmann, T., 2004. A Fenton reaction at the endoplasmic reticulum is involved in the redox control of hypoxia-inducible gene expression. *Proc. Natl. Acad. Sci.* 101, 4302–4307. <https://doi.org/10.1073/pnas.0400265101>
- Liu, W., Huang, J., Lin, Y., Cai, C., Zhao, Y., Teng, Y., Mo, J., Xue, L., Liu, L., Xu, W., Guo, X., Zhang, Y., Zhang, J. (Jim), 2020. Negative ions offset cardiorespiratory benefits of PM 2.5 reduction from residential use of negative ion air purifiers. *Indoor Air* 12728. <https://doi.org/10.1111/ina.12728>
- Lucas, M.S., Dias, A.A., Sampaio, A., Amaral, C., Peres, J.A., 2007. Degradation of a textile reactive Azo dye by a combined chemical–biological process: Fenton’s reagent-yeast. *Water Res.* 41, 1103–1109. <https://doi.org/10.1016/j.watres.2006.12.013>
- Mallapaty, S., 2020. How sewage could reveal true scale of coronavirus outbreak. *Nature.* <https://doi.org/10.1038/d41586-020-00973-x>
- Mao, K., Zhang, H., Yang, Z., 2020. Can a Paper-Based Device Trace COVID-19 Sources with Wastewater-Based Epidemiology? *Environ. Sci. Technol.* 54, 3733–3735. <https://doi.org/10.1021/acs.est.0c01174>
- Martí, M., Tuñón-Molina, A., Aachmann, F.L., Muramoto, Y., Noda, T., Takayama, K., Serrano-Aroca, Á., 2021. Protective Face Mask Filter Capable of Inactivating SARS-CoV-2, and Methicillin-Resistant *Staphylococcus aureus* and *Staphylococcus epidermidis*. *Polymers (Basel)*. 13, 207. <https://doi.org/10.3390/polym13020207>
- Miaskiewicz-Peska, E., Lebkowska, M., 2012. Comparison of aerosol and bioaerosol collection on air filters. *Aerobiologia (Bologna)*. 28, 185–193. <https://doi.org/10.1007/s10453-011-9223-1>
- Morawska, L., Cao, J., 2020. Airborne transmission of SARS-CoV-2: The world should face the reality. *Environ. Int.* 139, 105730. <https://doi.org/10.1016/j.envint.2020.105730>
- Morawska, L., Tang, J.W., Bahnfleth, W., Bluysen, P.M., Boerstra, A., Buonanno, G.,

- Cao, J., Dancer, S., Floto, A., Franchimon, F., Haworth, C., Hogeling, J., Isaxon, C., Jimenez, J.L., Kurnitski, J., Li, Y., Loomans, M., Marks, G., Marr, L.C., Mazzarella, L., Melikov, A.K., Miller, S., Milton, D.K., Nazaroff, W., Nielsen, P. V., Noakes, C., Peccia, J., Querol, X., Sekhar, C., Seppänen, O., Tanabe, S., Tellier, R., Tham, K.W., Wargocki, P., Wierzbicka, A., Yao, M., 2020. How can airborne transmission of COVID-19 indoors be minimised? *Environ. Int.* 142, 105832. <https://doi.org/10.1016/j.envint.2020.105832>
- National Academies of Sciences, 2020. Rapid Expert Consultation on SARS-CoV-2 Survival in Relation to Temperature and Humidity and Potential for Seasonality for the COVID-19 Pandemic (April 7, 2020). National Academies Press, Washington, D.C. <https://doi.org/10.17226/25771>
- Nissen, K., Krambrich, J., Akaberi, D., Hoffman, T., Ling, J., Lundkvist, Å., Svensson, L., Salaneck, E., 2020. Long-distance airborne dispersal of SARS-CoV-2 in COVID-19 wards. *Sci. Rep.* 10, 19589. <https://doi.org/10.1038/s41598-020-76442-2>
- Noorimotlagh, Z., Jaafarzadeh, N., Martínez, S.S., Mirzaee, S.A., 2021. A systematic review of possible airborne transmission of the COVID-19 virus (SARS-CoV-2) in the indoor air environment. *Environ. Res.* 193, 110612. <https://doi.org/10.1016/j.envres.2020.110612>
- Phan, T., 2020. Genetic diversity and evolution of SARS-CoV-2. *Infect. Genet. Evol.* 81, 104260. <https://doi.org/10.1016/j.meegid.2020.104260>
- Prather, K.A., Marr, L.C., Schooley, R.T., McDiarmid, M.A., Wilson, M.E., Milton, D.K., 2020. Airborne transmission of SARS-CoV-2. *Science* (80-.). eabf0521. <https://doi.org/10.1126/science.abf0521>
- Sahin, A.R., 2020. 2019 Novel Coronavirus (COVID-19) Outbreak: A Review of the Current Literature. *Eurasian J. Med. Oncol.* 7. <https://doi.org/10.14744/ejmo.2020.12220>
- Salussoglia, A.I.P., de Souza, C.W.O., Tanabe, E.H., Lopes Aguiar, M., 2020. Evaluation of filter media covered with spun fibres and containing thyme essential oil with antimicrobial properties. *Environ. Technol.* 1–10. <https://doi.org/10.1080/09593330.2020.1786167>
- Seader, J., Henley, J.E., Roper, D.K., 2011. SEPARATION PROCESS PRINCIPLES: Chemical and Biochemical Operations, 3rd-rd ed. John Wiley & Sons, Inc.
- Shalal, A., Lawder, D., 2020. IMF sees pandemic causing global recession in 2020, recovery in 2021 [WWW Document]. Reuters. URL <https://www.reuters.com/article/us-health-coronavirus-imf/imf-sees-pandemic-causing-global-recession-in-2020-recovery-in-2021-idUSKBN21A330> (accessed 3.29.20).
- Shishkin, A., Aguedal, H., Goel, G., Peculevica, J., Newport, D., Ozolins, J., 2020a. Influence of waste glass in the foaming process of open cell porous ceramic as filtration media for industrial wastewater. *J. Clean. Prod.* 124546. <https://doi.org/10.1016/j.jclepro.2020.124546>
- Shishkin, A., Baronins, J., Mironovs, V., Lukáč, F., Štubňa, I., Ozolins, J., 2020b. Influence of Glass Additions on Illitic Clay Ceramics. *Materials* (Basel). 13, 596. <https://doi.org/10.3390/ma13030596>
- Shishkin, A., Korjakins, A., Mironovs, V., 2015. Using of Cavitation Disperser, for Porous Ceramic and Concrete Material Preparation. *Int. J. Environ. Chem. Ecol. Geol.*

- Geophys. Eng. 9, 511–515.
- Shishkin, A., Laksa, A., Shidlovska, V., Timermane, Z., Aguedal, H., Mironovs, V., Ozolins, J., 2016. Illite Clay Ceramic Hollow Sphere - Obtaining and Properties. *Key Eng. Mater.* 721, 316–321. <https://doi.org/10.4028/www.scientific.net/KEM.721.316>
- Singh, A.K., Singh, A., Shaikh, A., Singh, R., Misra, A., 2020. Chloroquine and hydroxychloroquine in the treatment of COVID-19 with or without diabetes: A systematic search and a narrative review with a special reference to India and other developing countries. *Diabetes Metab. Syndr. Clin. Res. Rev.* 14, 241–246. <https://doi.org/10.1016/j.dsx.2020.03.011>
- Singh, R., Adhikari, R., 2020. Age-structured impact of social distancing on the COVID-19 epidemic in India.
- Song, I.H., Kim, M.J., Kim, H.D., Kim, Y.W., 2006. Processing of microcellular cordierite ceramics from a preceramic polymer. *Scr. Mater.* 54, 1521–1525. <https://doi.org/10.1016/j.scriptamat.2005.12.039>
- Soret, R., Fanlo, J.-L., Malhautier, L., Geiger, P., Bayle, S., 2018. Investigation of Removal Capacities of Biofilters for Airborne Viable Micro-Organisms. *Int. J. Environ. Res. Public Health* 15, 551. <https://doi.org/10.3390/ijerph15030551>
- Srivastava, A., 2021. COVID-19 and air pollution and meteorology-an intricate relationship: A review. *Chemosphere* 263, 128297. <https://doi.org/10.1016/j.chemosphere.2020.128297>
- Stanford, M.G., Li, J.T., Chen, Y., McHugh, E.A., Liopo, A., Xiao, H., Tour, J.M., 2019. Self-Sterilizing Laser-Induced Graphene Bacterial Air Filter. *ACS Nano* 13, 11912–11920. <https://doi.org/10.1021/acsnano.9b05983>
- Svinka, R., Svinka, V., Zake, I., 2011. Silica containing highly porous alumina ceramic. *IOP Conf. Ser. Mater. Sci. Eng.* 18, 182008. <https://doi.org/10.1088/1757-899X/18/18/182008>
- van Doremalen, N., Bushmaker, T., Morris, D.H., Holbrook, M.G., Gamble, A., Williamson, B.N., Tamin, A., Harcourt, J.L., Thornburg, N.J., Gerber, S.I., Lloyd-Smith, J.O., de Wit, E., Munster, V.J., 2020. Aerosol and Surface Stability of SARS-CoV-2 as Compared with SARS-CoV-1. *N. Engl. J. Med.* 382, 1564–1567. <https://doi.org/10.1056/NEJMc2004973>
- Walsh, N.P., Cotovio, V., 2020. Bats are not to blame for coronavirus. Humans are [WWW Document]. *CNN*. URL <https://edition.cnn.com/2020/03/19/health/coronavirus-human-actions-intl/index.html> (accessed 3.29.20).
- Wang, C., Xi, J.-Y., Hu, H.-Y., Yao, Y., 2009. Advantages of combined UV photodegradation and biofiltration processes to treat gaseous chlorobenzene. *J. Hazard. Mater.* 171, 1120–1125. <https://doi.org/10.1016/j.jhazmat.2009.06.129>
- Wang, Y., Sun, Y., Li, W., Tian, W., Irini, A., 2015. High performance of nanoscaled Fe₂O₃ catalyzing UV-Fenton under neutral condition with a low stoichiometry of H₂O₂: Kinetic study and mechanism. *Chem. Eng. J.* 267, 1–8. <https://doi.org/10.1016/j.cej.2014.08.016>
- Wardman, P., Candeias, L.P., 1996. Fenton Chemistry: An Introduction. *Radiat. Res.* 145, 523. <https://doi.org/10.2307/3579270>
- Worldometer, 2021. COVID-19 Coronavirus Pandemic [WWW Document]. Worldometer. URL <https://www.worldometers.info/coronavirus/>
- Wu, B., Zhang, S., He, S., Xiong, Y., 2019. Follow-up mechanism study on NO oxidation

- with vaporized H₂O₂ catalyzed by Fe₂O₃ in a fixed-bed reactor. *Chem. Eng. J.* 356, 662–672. <https://doi.org/10.1016/j.cej.2018.09.041>
- Zake-Tiluga, I., Svinka, R., Svinka, V., 2014. Highly porous corundum-mullite ceramics - Structure and properties. *Ceram. Int.* 40, 3071–3077. <https://doi.org/10.1016/j.ceramint.2013.09.139>
- Zake-Tiluga, I., Svinka, V., Svinka, R., Grase, L., 2015. Thermal shock resistance of porous Al₂O₃-mullite ceramics. *Ceram. Int.* 41, 11504–11509. <https://doi.org/10.1016/j.ceramint.2015.05.116>
- Zhou, P., Yang, X.-L., Wang, X.-G., Hu, B., Zhang, L., Zhang, W., Si, H.-R., Zhu, Y., Li, B., Huang, C.-L., Chen, H.-D., Chen, J., Luo, Y., Guo, H., Jiang, R.-D., Liu, M.-Q., Chen, Y., Shen, X.-R., Wang, X., Zheng, X.-S., Zhao, K., Chen, Q.-J., Deng, F., Liu, L.-L., Yan, B., Zhan, F.-X., Wang, Y.-Y., Xiao, G.-F., Shi, Z.-L., 2020. A pneumonia outbreak associated with a new coronavirus of probable bat origin. *Nature* 579, 270–273. <https://doi.org/10.1038/s41586-020-2012-7>
- Zhou, W., Yan, W., Li, N., Li, Y., Dai, Y., Han, B., Wei, Y., 2018. Preparation and characterization of mullite foam ceramics with porous struts from white clay and industrial alumina. *Ceram. Int.* 44, 22950–22956. <https://doi.org/10.1016/j.ceramint.2018.09.092>